Journal of Power Sources, *28* (1989) 301 - 315

SIMULATION STUDIES ON THE PERFORMANCE OF THE HYDROGEN ELECTRODE BONDED TO PROTON EXCHANGE MEMBRANES IN THE HYDROGEN–BROMINE FUEL CELL

S. D. FRITTS and R. F. SAVINELL*

Department of Chemical Engineering, Case Western Reserve University, Cleveland, OH 44106 (U.S.A.)

(Received February 22, 1989; in revised form August 2, 1989)

Summary

A mathematical model was developed to describe the performance of hydrogen electrode catalyst particles that are bonded to the proton exchange membrane of a hydrogen–bromine fuel cell. Macrohomogeneous porous electrode theory was applied to the catalyst particles. Fundamental equations were used to describe the transport of protons and dissolved hydrogen in the catalyst zone. The distribution of the electrode particles in this zone was also included in the model. Parametric studies on the numerical solution to this model indicate that the performance of the membrane electrode assembly is optimized when the volume fraction of polymer and catalyst is equal in the catalyst zone.

Introduction

Proton exchange membranes, (PEMs) that have platinum catalyst particles bonded to them are used in hydrogen–bromine fuel cells, hydrogen–chlorine fuel cells, SPE (H_2–O_2) fuel cells, SPE water electrolyzers, and in some electro-organic syntheses [1 - 5]. In these systems, the PEM acts as both a separator and as the electrolyte. When an electrode is bonded to a PEM, gaseous species can directly undergo an electrode reaction without additional electrolyte. A primary advantage of the catalyzed membrane is that bonding of the electrode to the membrane ensures the direct contact necessary for adequate transport of cations and electrons.

In this research we modelled the performance of these catalyzed membranes, referred to as the membrane electrode assembly (MEA). The specific application of our work is the rechargeable hydrogen–bromine fuel cell. The hydrogen half-cell is a gaseous hydrogen phase in contact with the MEA. The bromine half-cell contains a porous flow-by electrode through which aqueous hydrobromic acid and bromine flow. During discharge, hydrogen gas dissolves into the membrane and diffuses to the catalyst

*Author to whom correspondence should be addressed.

0378-7753/89/$3.50 © Elsevier Sequoia/Printed in The Netherlands

particles where it is oxidized to form protons. The protons are transported through the PEM to the aqueous bromine half-cell, where bromine is reduced to bromide ions. Nafion is typically used as the PEM in H_2–Br_2 fuel cells.

The functional groups in a Nafion membrane are believed to be in the form of ion clusters [6, 7]. In these clusters, the polymeric ions and the absorbed electrolyte phase separate from the fluorocarbon backbone into spherical clusters connected by short, narrow channels [6]. Protons are associated with the fixed, functional polymeric groups and with the free water phase, and are transported through the membrane via a migration/diffusion mechanism. Ogumi *et al.* [8] concluded from hydrogen solubility data in Nafion and PTFE that permeation of gases takes place in the fluorocarbon backbone.

In an earlier communciation [9] we reported results of charge and discharge modelling of the hydrogen–bromine fuel cell system to determine the effects of kinetics, mass transfer, and cell design on single-cell performance. The hydrogen electrode was assumed to be a planar electrode with extended surface area that was bonded to the PEM. Proton transport across the membrane was described by a diffusion–migration mechanism, assuming a linear concentration gradient. The results of that modelling effort indicated that there were optimum specific surface areas for both the hydrogen and bromine electrodes. Also, the modelling work indicated that membrane properties such as proton diffusion and concentration had the greatest effect on the cell performance.

A detailed modelling study of the MEA was therefore initiated to examine the effects of mass transfer, kinetics, and the distribution of the catalyst loading. Some results of this modelling effort are reported here.

Model development

A schematic of the MEA model system is shown in Fig. 1. The Figure depicts a closely packed arrangement of platinum particles at the edge of the membrane, and a looser arrangement of platinum particles deeper in the catalyst zone. One method of preparing MEAs is to hot-press a mixture of platinum and solubilized Nafion onto a Nafion film, which gives this type of catalyst distribution. In this work a linear equation was assumed to describe the distribution of platinum volume fraction in the catalyst zone for computational ease. Also, the performance of the MEA was simulated for a uniform catalyst distribution.

Macro-homogeneous porous electrode theory [10, 11] was used to describe the electrode formed by the catalyst particles that are bonded to the membrane. In this model, two phases are assumed to exist in the catalyst zone. The polymer phase is assumed to be a continuum of the fluorocarbon backbone, polymeric ions, and absorbed electrolyte phases of the PEM. The parameters used to describe the transport in the Nafion are those reported elsewhere for hydrated Nafion [1, 4, 7, 12]. The second phase is

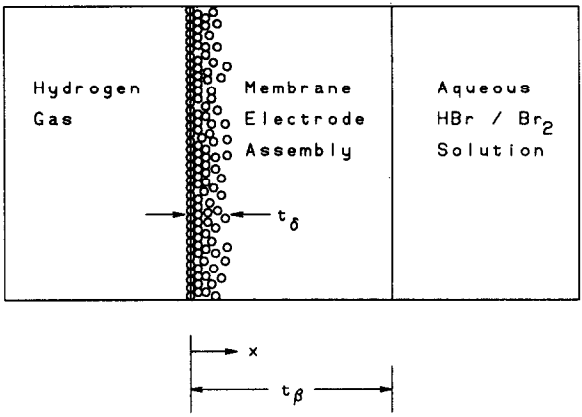

Fig. 1. Schematic of membrane electrode assembly.

the platinum particles that are dispersed throughout the catalyst zone. The basis of the model and the resulting equations are now presented. The particles are assumed to be platinum spheres with an electrochemically active surface area of

$$a = \frac{3}{r_p}(1-\epsilon) \tag{1}$$

The nomenclature is presented at the end of this paper. The diffusion of dissolved hydrogen to the catalyst particles and its subsequent reaction can be described by the following expression

$$ai'' = 2FD_{H_2}\frac{d}{dx}\left(\epsilon\frac{dC_{H_2}}{dx}\right) \tag{2}$$

where i'' is the local current density on the particles. The boundary conditions for eqn. (2) are:

$$x = 0, \qquad C_{H_2} = C^{o}_{H_2} \tag{3}$$

$$x = t_\delta, \qquad \epsilon\frac{dC_{H_2}}{dx} = \frac{C_{H_2}}{t_\beta - t_\delta} \tag{4}$$

In eqn. (4) the left hand side represents the flux of hydrogen through the catalyst zone while the right hand side represents the flux through the remaining catalyst-free polymer film. It is assumed that the hydrogen concentration in the solution phase adjacent to the membrane is negligible.

In the PEM, there are protons associated with the fixed functional groups that migrate through the MEA, as well as protons in the free acid phase that diffuse through the membrane. The transport of protons in the membrane is described with a diffusion/migration mechanism which can be expressed as

$$ai'' = -FD_{H^+}\frac{d}{dx}\left(\epsilon\frac{dC_{H^+}}{dx}\right) - F^2u_{H^+}\frac{d}{dx}\left(\epsilon C_{H^+}\frac{d\phi_2'}{dx}\right) \tag{5}$$

with boundary conditions on concentration of

$$x = 0, \qquad \frac{dC_{H^+}}{dx} = 0 \tag{6}$$

$$x = t_\delta, \qquad C_{H^+} = C^o_{H^+} \tag{7}$$

Transport of water through the membrane was not considered to be a major problem in the hydrogen–bromine fuel cell, since the membrane is in contact with the aqueous hydrobromic acid solution, so drying effects should not be severe. However, since the water concentration in the Nafion film decreases with increasing acid concentration [13], if the local hydrogen ion concentration becomes too high there may not be enough water molecules associated with the hydrogen ion for proton transport. The concentration of water in the membrane was estimated [13] to be 30% at the highest local proton concentration in the membrane and 31% at the lowest local proton concentration. These estimates indicate that the transport of water in the membrane is not expected to have a major impact on cell performance.

The potential distribution in the catalyst zone is described by the charge balance, shown as eqn. (8). It was assumed that the diffusion coefficients for hydrogen ions and bromide ions are equal.

$$ai'' = -\kappa\frac{d}{dx}\left(\epsilon\frac{d\phi_2'}{dx}\right) \tag{8}$$

The boundary conditions for the charge balance are:

$$x = 0, \qquad \frac{d\phi_2'}{dx} = 0 \tag{9}$$

$$x = t_\delta, \qquad \phi_2' = \phi_2'^{o} \tag{10}$$

In the balance equations (eqns. (2), (5), and (8)), the effective transport constants contain an explicit linear dependency on ϵ. The terms ϵD_{H_2}, ϵD_{H^+}, ϵu_{H^+}, and $\epsilon\kappa$ are all effective constants which take into account porosity as well as tortuosity [11].

A Butler–Volmer form of kinetic expression is used to represent the interfacial reaction rates.

$$i'' = i''_{o,ref}\left[\left(\frac{C_{H_2}}{1\ \text{atm}/R'T}\right)^{1/2}\exp\left\{\frac{\alpha_a F}{RT}(\phi_1' - \phi_2')\right\} - \frac{C_{H^+}}{1\ \text{mol/l}}\exp\left\{\frac{-\alpha_c F}{RT}(\phi_1' - \phi_2')\right\}\right] \tag{11}$$

Simulation studies were performed to determine the effect of a non-uniform metal phase potential for the case where the platinum catalyst

distribution is uniform. In this case, the metal phase charge balance can be written as

$$ai'' = \sigma_o(1-\epsilon)^{1.5}\frac{d^2\phi_1'}{dx^2} \tag{12}$$

with boundary conditions

$$x = 0, \qquad \phi_1' = V \tag{13}$$

$$x = t_\delta, \qquad \frac{d\phi_1'}{dx} = 0 \tag{14}$$

The effective conductivity used in eqn. (12) was developed by Bruggeman [14] for a continuous conducting phase, and its use here is an approximation.

Simulation results

The equations of the model described in the previous section were made dimensionless. Scheme 1 shows the dimensionless equations used to model the MEA when the platinum distribution is non-uniform in the catalyst zone. The parameters used in the dimensionless equations are given in Scheme 2.

The magnitude of the dimensionless parameters *PA*, *PB*, *PC* represent the magnitude of the gradients of potential, dissolved hydrogen, and protons. The ratio of these parameters indicates the predominance of a controlling resistance. For example, the ratio *PB*/*PA* represents the ratio of hydrogen diffusion resistance to ohmic resistance. The other parameters, *PD*, *PE*, *Q* represent dimensionless forms of the exchange current density, metal phase potential, and catalyst penetration into the polymer membrane.

Examining the dimensionless equations in Scheme 1, one sees that the balance equations include a $(1-\epsilon)$ term on the left hand side while the kinetic expression does not. This implies that as the polymer volume fraction increases, the kinetic resistances become larger relative to the effects of transport gradients.

The dimensionless equations were cast into finite difference form. The resulting matrix was solved using the BAND program, an iterative, implicit method developed by Newman [15]. The computer simulations were performed on a DSI-780 board of Definicon Systems, on an IBM-XT computer.

The base case parameters used in the simulations are given in Scheme 3. The mobility of the protons in the membrane was estimated from the conductivity data reported by Yeo and Chin [1]. Then, the Nernst–Einstein relationship was used to estimate the diffusion coefficient of protons in the membrane. The solubility of hydrogen in the membrane, $C^o_{H_2}$, was calculated from the hydrogen permeability data at 100 °F and 150 psi of Nuttall [4], using the H_2 diffusion coefficient determined by Yeo and McBreen [12].

Proton mass balance

$$PC(1-\epsilon)C_4 = -\left(\epsilon \frac{dC_1}{dX}\frac{dC_3}{dX} + C_1 \frac{d\epsilon}{dX}\frac{dC_3}{dX} + C_1\epsilon \frac{d^2C_3}{dX^2}\right) - \frac{1}{\alpha}\left(\frac{d\epsilon}{dx}\frac{dC_1}{dX} + \epsilon \frac{d^2C_1}{dX}\right)$$

Hydrogen mass balance

$$PB(1-\epsilon)C_2 = \frac{d\epsilon}{dX}\frac{dC_2}{dX} + \epsilon \frac{d^2C_2}{dX^2}$$

Charge balance

$$-PA(1-\epsilon)C_4 = \frac{d\epsilon}{dX}\frac{dC_3}{dX} + \epsilon \frac{d^2C_3}{dX^2}$$

Kinetic expression

$$PDC_4 = C_2^{1/2}\exp(PE - C_3) - C_1\exp(C_3 - PE)$$

Boundary conditions

$$X = 0, \qquad \frac{dC_1}{dX} = 0, \qquad C_2 = C_2^{\circ}, \qquad \frac{dC_3}{dX} = 0$$

$$X = 1, \qquad C_1 = C_1^{\circ}, \qquad C_2 = Q\frac{dC_2}{dX}, \qquad C_3 = C_3^{\circ}$$

Scheme 1. Dimensionless equations used to model the catalyst zone of the membrane electrode assembly for a non-uniform distribution of platinum particles in the catalyst zone.

Variables

$$C_1 = \frac{C_{H^+}}{1\ \text{mol l}^{-1}}, \qquad C_2 = \frac{C_{H_2}}{1\ \text{atm}(R'T)^{-1}}, \qquad C_3 = \frac{\alpha F\phi_2'}{RT},$$

$$C_4 = \frac{i''}{1\ \text{A cm}^{-2}} \qquad X = \frac{x}{t_\delta}$$

Parameters

$$PA = \frac{3\alpha F(1\ \text{A/cm}^2)t_\delta{}^2}{\kappa RTr_p}, \qquad PB = \frac{3(1\ \text{A/cm}^2)t_\delta{}^2R'T}{2r_pD_{H_2}F(0.001\ \text{mol cm}^{-3})}$$

$$PC = \frac{3(1\ \text{A/cm}^2)t_\delta{}^2}{r_pD_{H^+}F(0.001\ \text{mol cm}^{-3})}, \qquad PD = \frac{1\ \text{A/cm}^2}{i''_{o,\text{ref}}}$$

$$PE = \frac{\alpha F\phi_1'}{RT}, \qquad Q = \epsilon\frac{t_\beta - t_\delta}{t_\delta}$$

Scheme 2. Definitions used in the dimensionless equations of Table 1.

$D_{H_2} = 6.6 \times 10^{-7}\ cm^2\ s^{-1}$ [12]

$D_{H^+} = 9.8 \times 10^{-7}\ cm^2\ s^{-1}$ [1]

$C^o_{H^+} = 6.8\ mol\ l^{-1}$ [1]

$C^o_{H_2} = 0.59\ mol\ l^{-1}$ [4, 12]

$r_p = 0.5 \times 10^{-6}$ cm

$t_\beta = 0.025$ cm [1]

$\kappa = 0.05$ mho cm^{-1} [1]

$t_\delta = 9.35 \times 10^{-5}$ cm

$T = 298$ K

$i''_{o,ref} = 0.001\ A\ cm^{-2}$

$(V - \phi'_2)|_{x=t_\delta} = 0.05$ V

$PA = 20.43$

$PB = 1007.1$

$PC = 554.7$

$PD = 1000$

$PE = 0$

Scheme 3. Base case parameters used in the simulations.

The proton concentration in the membrane was estimated from the data of Yeo and Chin [1]. A platinum particle diameter of 100 Å was used in the simulations [16] with an exchange current density of 1 mA cm^{-2}, a typical value for hydrogen evolution on platinum [19].

For the base case studies, the platinum loading was 1 mg cm^{-2}. The thickness of the catalyst zone, t_β, was estimated from the catalyst loading and the fraction of the catalyst zone that is filled with catalyst $(1 - \epsilon)$. The base case dimensionless parameters are given in Scheme 3. As indicated by the magnitudes of PA, PB and PC, the potential gradient across the catalyst zone is small relative to the gradients of hydrogen and proton concentration. The distributions of the dimensionless potential, hydrogen concentration, and proton concentration for the base case are shown in Fig. 2.

Further sensitivities of the dimensionless parameters are demonstrated in Table 1. The last column of this Table represents the integration of C_4 over the catalyst zone. Multiplying this quantity by $3t_\delta/r_p$ will give i', the current density based on PEM geometric area. In row 1 of Table 1 is shown the calculation result for the base case. In row 2, only PB is decreased by an order of magnitude (*i.e.*, an increase in H_2 diffusion coefficient). In row 3, both PA and PC are decreased by an order of magnitude (*i.e.*, an increase in proton mobility). Both cases show only a marginal effect on electrode performance. However, in row 4, one sees the effect of intrinsic catalyst activity for the otherwise base case, which is sizable. In row 5, PA, PB and PC are all increased by an order of magnitude (*i.e.*, t_δ^2/r_p increases). Recalling that i' is obtained by multiplying the last column by $3t_\delta/r_p$, one sees that the effect is significant. However, as shown in row 6, the effects of intrinsic catalytic activity is not as great when t_δ^2/r_p becomes larger.

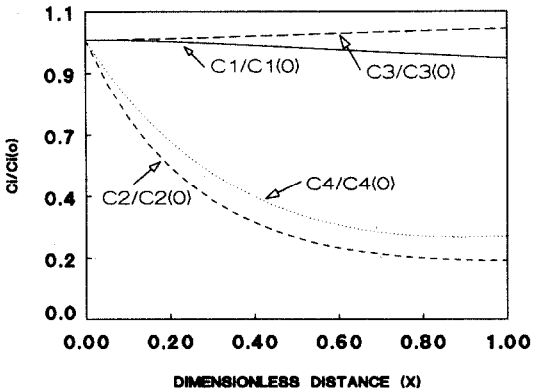

Fig. 2. Distributions of the dimensionless variables relative to the value at $X = 0$ for the base case: $C_1(0) = 7.316$; $C_2(0) = 14.33$; $C_3(0) = -0.936$; $C_4(0) = 0.006\,79$.

TABLE 1

Electrode performance sensitivity to dimensionless parameters

Row	*PA*	*PB*	*PC*	*PD*	$\int_0^1 C_4\,\mathrm{d}X$
1	[a]	[a]	[a]	[a]	0.0027
2	[a]	100.71	[a]	[a]	0.0029
3	2.043	[a]	55.47	[a]	0.0029
4	[a]	[a]	[a]	100	0.0109
5	204.3	10071	5547	[a]	0.0011
6	204.3	10071	5547	100	0.0016

[a]Value for the base case.

To provide a more physical feel for the calculation results, further analysis is reported for dimensional quantities. Simulations of charge and discharge reactions were performed for a linear platinum distribution described by the expression

$$\epsilon = 0.32 + 0.48\,\frac{x}{t_\delta} \tag{15}$$

The local current density and dissolved hydrogen concentrations for the discharge reaction are shown in Fig. 3. The current density is largest at the gas phase/MEA interface, and it decreases rapidly into the catalyst zone. The dissolved hydrogen concentration follows a similar profile, but with a steeper gradient near the gas phase/MEA interface. The dissolved hydrogen concentration and current distributions suggest that the reaction is limited by the diffusion of dissolved hydrogen into the dense catalyst region at the gas phase/MEA interface.

The magnitude of the local current density and the local dissolved hydrogen concentration profiles for the charge reaction are shown in Fig. 4. The current density shows a minimum near the gas phase/MEA interface and

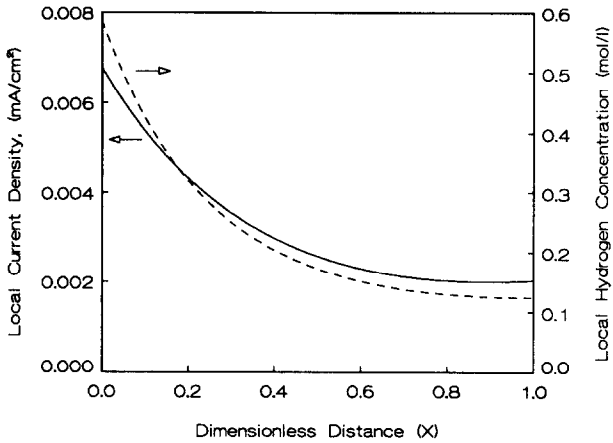

Fig. 3. Predicted local current densities and dissolved hydrogen concentrations for the simulated discharge reaction.

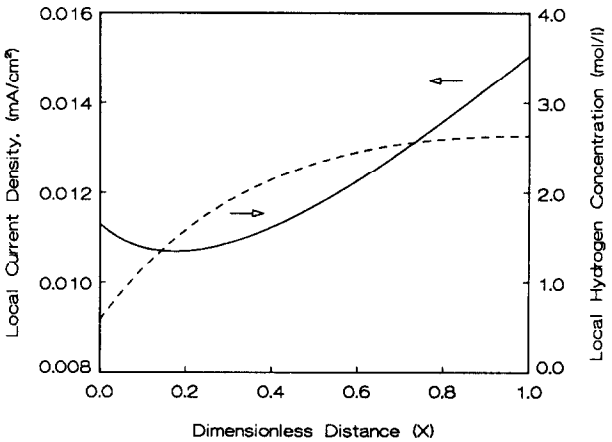

Fig. 4. Predicted magnitude of the local current densities and the local dissolved hydrogen concentrations for the simulated charge reaction.

has a maximum at the edge of the catalyst zone. Although the current increases about fifty percent. across the catalyst zone, the dissolved hydrogen concentration increases nearly three hundred percent. This demonstrates that slow dissolved hydrogen diffusion causes a substantial build-up of dissolved hydrogen deep within the catalyst zone. Consequently, in practice, it may be necessary to charge the cell slowly to avoid rupturing the membrane due to hydrogen phase-change.

The local current densities as shown in Figs. 3 and 4 for the reactions appear to be low because they are based on the high specific surface areas of the catalysts, ranging from 4.1×10^6 cm^2 cm^{-3} at the gas phase/MEA interface to 1.2×10^6 cm^2 cm^{-3} at the edge of the catalyst zone. The current

density based on apparent PEM geometric electrode area can be calculated by

$$i' = a\int_0^{t_\delta} i''\,dx \tag{16}$$

where the integral was estimated numerically in this work, using the trapezoidal rule.

The effect of a non-uniform metal phase potential (eqn. (12)) was examined. When electrode structures are composed of a collection of solid particles, a low and unpredictable value of the metal conductivity is observed due to contact resistance between the particles [17]. Metal phase conductivities of 9.26 - 92 600 mho cm^{-1} were used in the simulations. The difference in the predicted apparent current density between these extreme values of conductivities was less than 0.5% for a platinum loading of 1 mg cm^{-2}. This result demonstrates that the simpler model of assuming a uniform metal phase potential is reasonable for future simulations.

Additional calculations of MEA performance are reported as polarization curves. The reported driving forces are given as the potential of an H_2–Br_2 cell, less the overpotentials associated with the porous bromine electrode and less the ohmic resistance of the uncatalyzed portion of the membrane.

The performance of the MEA was simulated for both a linear platinum distribution within the PEM and for a uniform distribution of platinum particles. The linear platinum distribution is described by eqn. (15), and for the other case the polymer volume fraction is assumed to be 0.56. The total platinum loading in both cases is kept constant at 1 mg cm^{-2}. Simulated polarization curves for the discharge reaction are shown in Fig. 5. A uniform platinum distribution gives slightly better performance than an MEA with a linear platinum distribution. In the latter case, the dense packing of spheres at the MEA/gas phase interface somewhat restricts the diffusion of hydrogen gas into the catalyst zone. Other dependencies of effective transport constants on porosity may give a different result. However, as was shown earlier, the effect of conductivity on SPE base case performance is minimal. All other results reported here will be for the case of a uniform platinum distribution in the catalyst zone.

Simulated polarization curves demonstrating the effect of catalyst zone polymer fraction on the MEA performance are shown in Fig. 6. The platinum loading for all cases is kept at 1 mg cm^{-2}. The optimum catalyst/polymer ratio is 1:1. MEAs with polymer fractions that are much higher than 0.5 exhibit kinetically limited behavior, and those with polymer fractions much lower than 0.5 show diffusion limitations.

The effect of platinum particle diameter was examined. The results are shown in Fig. 7 for particle diameters of 50, 100 and 200 Å, and platinum loadings of 1 mg cm^{-2}. These calculations demonstrate that an increase or decrease in the catalyst particle size of a factor of two can have a large

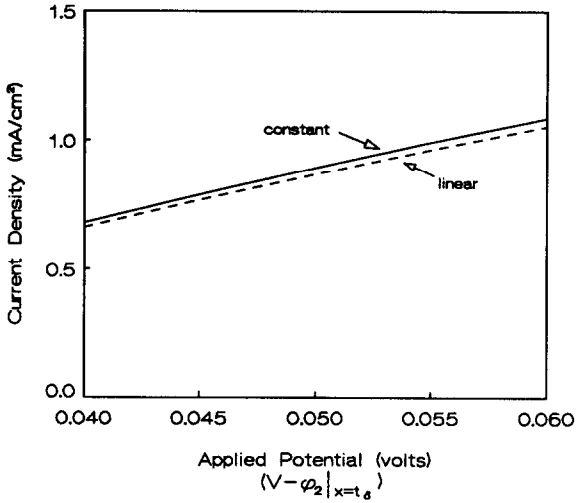

Fig. 5. Predicted MEA performance during discharge for linear and uniform catalyst distributions.

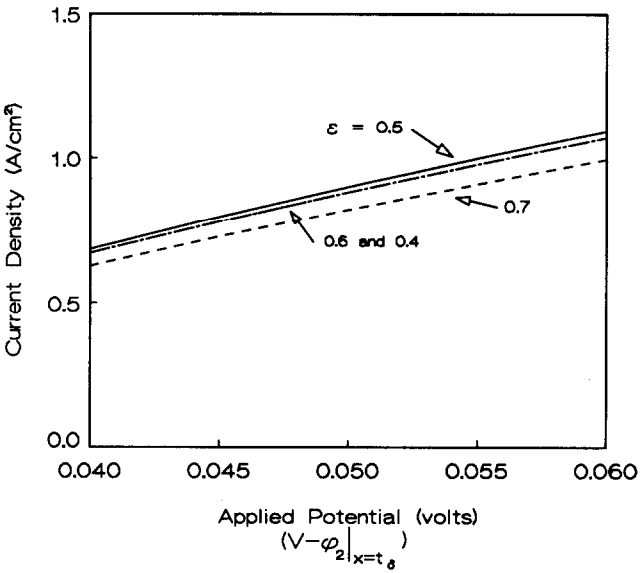

Fig. 6. Predicted MEA performance during discharge for polymer fractions in the catalyst zone of 0.4 - 0.7.

impact on MEA performance. Examining the dimensionless groups, the quantity t_δ^2/r_p is incorporated into *PA*, *PB* and *PC*, but not *PD*. Therefore, it can be seen that the kinetic resistance becomes less important as t_δ^2/r_p becomes larger. Also, examining eqn. (16), one can see that the current density based on apparent PEM geometric electrode area becomes greater as the ratio of t_δ/r_p increases.

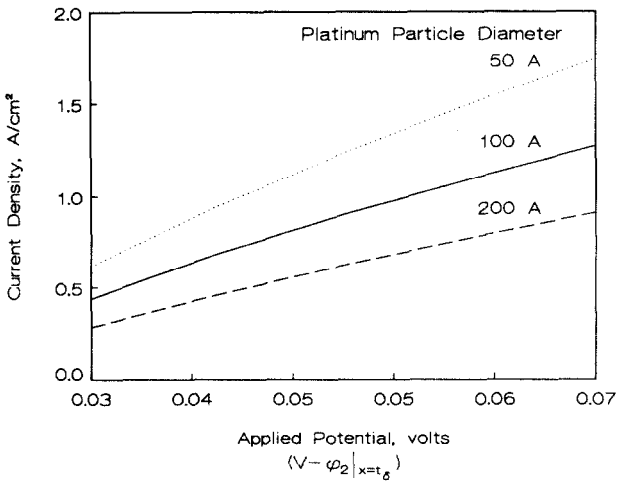

Fig. 7. Predicted MEA performance during discharge for platinum particle diameters of 50 - 100 Å.

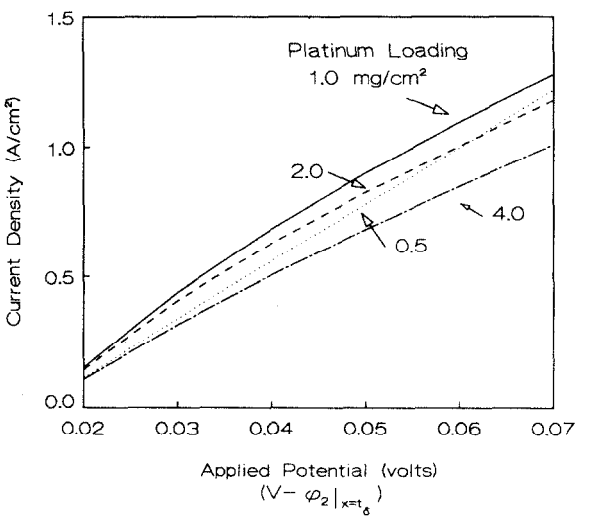

Fig. 8. Predicted MEA performance during discharge for platinum loadings ranging from 0.5 to 4.0 mg cm^{-2}.

The effect of platinum loading on MEA performance during discharge is shown in Fig. 8. MEAs with platinum loadings of 4.0, 2.0, 1.0, and 0.5 mg cm^{-2} were simulated for a polymer fraction, ϵ, of 0.5. The best performance occurs with the 1.0 mg cm^{-2} loading. The current densities are highest at the gas phase/membrane interface ($x = 0$). At high loadings the local current density decreases rapidly into the catalyst zone. Improved performance is achieved with an intermediate loading of 1 mg cm^{-2} because the local current density becomes more uniformly distributed in the catalyst zone.

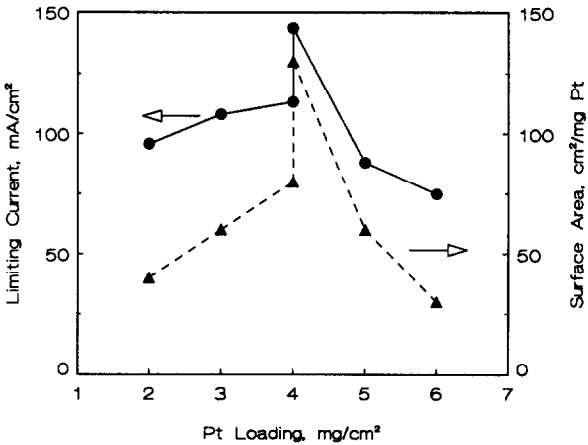

Fig. 9. Predicted hydrogen oxidation limiting current for comparison with the experimental data of ref. 16.

Fedkiw and Her [16] reported experimental data for the hydrogen oxidation reaction on MEAs prepared by an impregnation–reduction method. The authors reported the specific surface area of the MEA and the limiting current of hydrogen oxidation for several Pt loadings. MEA performance was simulated for similar Pt loadings and electrode specific surface areas, and the results are compared with their data. Since many details in their work were not available, a number of assumptions, including particle diameters, catalyst zone thickness, and void fractions had to be made [18]. In these simulations $C^{o}_{H_2}$ was assumed to be 0.0245 mole l^{-1} [12], since the experiments were performed at 1 atm hydrogen. The calculated results are shown in Fig. 9. The calculated currents show the same trends as were measured experimentally [16]. However, the magnitude of the currents differed significantly, probably because many of the parameters required for accurate comparison were not available and had to be estimated.

Conclusions

The model reported here is a useful tool for designing an optimally performing MEA. The structure of the catalyst zone has been shown to affect the performance of the MEA. Generally, the performance is kinetically limited. However, when the particles become densely packed, performance becomes gas diffusion limited.

The calculated results are based on estimates of a number of physical parameters, such as the concentrations of protons and hydrogen gas in the membrane, and the proton diffusion coefficient. Thus, experimental work is currently being done to measure some of these parameters using a.c. impedance techniques. This should improve the value of the model by allowing it to predict MEA performance more accurately.

Acknowledgements

The support of the NSF Grant CBT-8696073 is gratefully acknowledged. S.D.F. acknowledges the support of the Department of Energy for the Energy Research Summer Fellowship of the Electrochemical Society.

List of symbols

a	Electrochemically active surface area ($cm^2\ cm^{-3}$)
C_i	Concentration of species i ($mol\ cm^{-3}$)
C_1, C_2, C_3, C_4, X	Dimensionless variables defined in Scheme 2
D_i	Diffusion coefficient of species i ($cm^2\ s^{-1}$)
F	Faraday's constant (96 487 C equiv.$^{-1}$)
i''	Current density based on particle true area ($A\ cm^{-2}$)
$i''_{o,ref}$	Exchange current density at reference conditions based on particle true area ($A\ cm^{-2}$)
i'	Current density based on MEA apparent geometrical area ($A\ cm^{-2}$)
PA, PB, PC, PD, PE, Q	Dimensionless parameters defined in Scheme 2
r_p	Platinum particle radius (cm)
R	Gas constant (8.314 $J\ mol^{-1}\ K^{-1}$)
R'	Gas constant (0.082 05 l atm $K^{-1}\ mol^{-1}$)
T	Temperature (K)
t_β	Thickness of membrane (cm)
t_δ	Thickness of catalyst zone (cm)
u_{H^+}	Mobility of hydrogen ions ($cm^2\ mol\ (J\ s)^{-1}$)
x	Distance (cm)
$\alpha = \alpha_a = \alpha_c = 0.5$	Transfer coefficient
ϵ	Volume fraction of polymer in catalyst zone of the MEA
κ	Conductivity of PEM ($mho\ cm^{-1}$)
σ_o	Electronic conductivity of platinum particles ($mho\ cm^{-1}$)
ϕ'_1	Quasi-electrostatic potential of platinum particles (V)
ϕ'_2	Quasi-electrostatic potential in the polymer phase (V)

References

1 R. S. Yeo and D-T. Chin, *J. Electrochem. Soc.*, *127* (1980) 549.
2 R. S. Yeo, J. McBreen, A. C. C. Tseung and S. Srinivasan, *J. Appl. Electrochem.*, *10* (1980) 393.
3 A. Katayama-Aramata, H. Nakajima, K. Fujikawa and J. Kita, *Electrochim. Acta*, *28* (1983) 777.

4 L. J. Nuttall, *Int. J. Hydrogen Energy, 2* (1977) 395.
5 Z. Ogumi, K. Nishio and S. Yoshizawa, *Electrochim. Acta, 26* (1981) 1779.
6 W. Y. Hsu and T. D. Gierke, *J. Membrane Sci., 13* (1983) 307.
7 R. S. Yeo, *J. Electrochem. Soc., 130* (1983) 533.
8 Z. Ogumi, T. Kuhoe and Z. Takehara, *J. Electrochem. Soc., 132* (1985) 2601.
9 R. F. Savinell and S. D. Fritts, *J. Power Sources, 22* (1988) 423.
10 J. Newman and C. W. Tobias, *J. Electrochem. Soc., 109* (1962) 1183.
11 J. Newman and W. Tiedemann, *AIChE J., 21* (1975) 25.
12 R. S. Yeo and J. McBreen, *J. Electrochem. Soc., 126* (1979) 1682.
13 R. S. Yeo and H. L. Yeager, in B. E. Conway, R. E. White and J. O'M. Bockris (eds.), *Modern Aspects of Electrochemistry, 16*, Plenum Press, New York, 1985, p. 437.
14 C. A. G. Bruggeman, *Ann. Physik, 24* (1935) 636.
15 J. Newman, *Electrochemical Systems*, Prentice-Hall, NJ, 1973.
16 P. S. Fedkiw and W-H. Her, An impregnation reduction method to prepare electrodes on Nafion SPE, *J. Electrochem. Soc., 136* (1989) 899.
17 J. Newman and W. Tiedemann, in H. Gerischer and C. W. Tobias (eds.), *Advances in Electrochemistry and Electrochemical Engineering*, Vol. 11, Wiley, NY, 1985.
18 S. D. Fritts, *Ph.D. Thesis*, Case Western Reserve University, 1989.
19 J. O'M. Bockris and A. K. N. Reddy, *Modern Electrochemistry*, Vol. 2, Plenum Press, NY, 1970, p. 1238.